

# The nucleon spin and momentum decomposition using lattice QCD simulations

C. Alexandrou<sup>1,2</sup>, M. Constantinou<sup>3</sup>, K. Hadjiyiannakou<sup>1</sup>, K. Jansen<sup>4</sup>,

C. Kallidonis<sup>1</sup>, G. Koutsou<sup>1</sup>, A. Vaquero Avilés-Casco<sup>5</sup>, C. Wiese<sup>4</sup>

<sup>1</sup>*Computation-based Science and Technology Research Center,*

*The Cyprus Institute, 20 Kavafi Str., Nicosia 2121, Cyprus*

<sup>2</sup>*Department of Physics, University of Cyprus, P.O. Box 20537, 1678 Nicosia, Cyprus*

<sup>3</sup>*Department of Physics, Temple University, 1925 N. 12th Street, Philadelphia, PA 19122-1801, USA*

<sup>4</sup>*NIC, DESY, Platanenallee 6, D-15738 Zeuthen, Germany*

<sup>5</sup>*Department of Physics and Astronomy, University of Utah, Salt Lake City, UT 84112, USA*

We determine within lattice QCD, the nucleon spin carried by valence and sea quarks, and gluons. The calculation is performed using an ensemble of gauge configurations with two degenerate light quarks with mass fixed to approximately reproduce the physical pion mass. We find that the total angular momentum carried by the quarks in the nucleon is  $J_{u+d+s}=0.408(61)_{\text{stat.}}(48)_{\text{syst.}}$  and the gluon contribution is  $J_g=0.133(11)_{\text{stat.}}(14)_{\text{syst.}}$  giving a total of  $J_N=0.54(6)_{\text{stat.}}(5)_{\text{syst.}}$  consistent with the spin sum. For the quark intrinsic spin contribution we obtain  $\frac{1}{2}\Delta\Sigma_{u+d+s}=0.201(17)_{\text{stat.}}(5)_{\text{syst.}}$ . All quantities are given in the  $\overline{\text{MS}}$  scheme at 2 GeV. The quark and gluon momentum fractions are also computed and add up to  $\langle x \rangle_{u+d+s} + \langle x \rangle_g = 0.804(121)_{\text{stat.}}(95)_{\text{syst.}} + 0.267(12)_{\text{stat.}}(10)_{\text{syst.}} = 1.07(12)_{\text{stat.}}(10)_{\text{syst.}}$  satisfying the momentum sum.

PACS numbers:

*Introduction:* The distribution of the proton spin amongst its constituent quarks and gluons has been a long-standing puzzle ever since the European Muon Collaboration showed in 1987 that only a fraction of the proton spin is carried by the quarks [1, 2]. This was in sharp contrast to what one expected based on the quark model. This so-called “proton spin crisis” triggered a rich experimental and theoretical activity. Recent experiments show that only 30% of the proton spin is carried by the quarks [3], while experiments at RHIC [4, 5] on the determination of the gluon polarization in the proton point to a non-zero contribution [6]. A global fit to the most recent experimental data that includes the combined set of inclusive deep-inelastic scattering data (DIS) from HERA, and Drell-Yan data from Tevatron and LHC, led to an improved determination of the valence quark distributions and the flavor separation of the up- and down-quarks [7]. The combined HERA data also provide improved constraints on the gluon distributions but large uncertainties remain [7]. Obtaining the quark and gluon contributions to the nucleon spin and momentum fraction within lattice Quantum Chromodynamics (QCD) provides an independent input that is extremely crucial but the computation is very challenging. This is because a complete determination must include, besides the valence also sea quark and gluon contributions that exhibit a large noise-to-signal ratio and are computationally very demanding. A first computation of the gluon spin was performed recently via the evaluation of the gluon helicity in a mixed action approach of overlap valence quarks on  $N_f=2+1$  domain wall fermions that included an ensemble with pion mass 139 MeV [8]. In this work, we evaluate all the contributions to the spin of the proton as well as the gluon and quark momentum

fractions [9, 10]. Such an investigation has become feasible given the tremendous progress in simulating QCD on a Euclidean four-dimensional lattice with quark masses tuned to their physical values (referred to as the physical point) in combination with new approaches to evaluate sea quark and gluon contributions that were not possible in the past [9, 11–13]. This first study of valence and sea quark and gluon contributions directly at the physical point allows us to obtain a complete information on the distribution of the nucleon spin and momentum among its constituents.

*Computational approach:* We use one gauge ensemble employing two degenerate ( $N_f=2$ ) twisted mass clover-improved fermions [14, 15] with masses that approximately reproduce the physical pion mass [16] on a lattice of  $48^3 \times 96$  and lattice spacing  $a=0.0938(3)$  fm, determined from the nucleon mass [17]. The strange and charm valence quarks are taken as Osterwalder-Seiler fermions [18, 19]. The mass of the strange quark is tuned to reproduce the  $\Omega^-$  mass and the mass of the charm quark is tuned independently to reproduce the mass of  $\Lambda_c^+$  as described in detail in Ref. [17]. The strange and charm quark masses in lattice units determined through this matching are  $a\mu_s=0.0259(3)$  and  $a\mu_c=0.3319(15)$ , respectively, yielding  $\mu_c/\mu_s=12.8(2)$ . We note that if instead we tune to the ratio of the kaon (D-meson) to pion mass  $m_K/m_\pi$  ( $m_D/m_\pi$ ) for the same ensemble we find  $\mu_c/\mu_s=12.3(1)$  [16]. Given that an extrapolation to the continuum, where the different definitions are expected to be consistent, is not carried out and the errors quoted are only statistical, this level of agreement is very satisfactory. For the renormalized strange and charm quark masses we find  $m_s^R=\mu_s/Z_P=108.6(2.2)(5.7)(2.6)$  MeV and  $m_c^R=\mu_c/Z_P=1.39(2)(7)(3)$  GeV, where  $Z_P$  is the

pseudoscalar renormalization function determined non-perturbatively in the  $\overline{\text{MS}}$  at 2 GeV [17].

*Matrix elements:* We use Ji's sum rule [20], that provides a gauge invariant decomposition of the nucleon spin as

$$J_N = \sum_{q=u,d,s,c,\dots} \left( \frac{1}{2} \Delta \Sigma_q + L_q \right) + J_g,$$

where  $\frac{1}{2} \Delta \Sigma_q$  is the contribution from the intrinsic quark spin,  $L_q$  the quark orbital angular momentum and  $J_g$  is the gluon total angular momentum. The quark intrinsic spin  $\frac{1}{2} \Delta \Sigma_q$  is obtained from the first Mellin moment of the polarized parton distribution function (PDF), which is the nucleon matrix element of the axial-vector operator. The total quark angular momentum,  $J_q$ , can be extracted by computing the second Mellin moment of the unpolarized nucleon PDF, which is the nucleon matrix element of the vector one-derivative operator at zero momentum transfer. These matrix elements in Euclidean space are given by

$$\begin{aligned} \langle N(p, s') | \mathcal{O}_A^\mu | N(p, s) \rangle &= \bar{u}_N(p, s') \left[ g_A^q \gamma^\mu \gamma_5 \right] u_N(p, s), \\ \langle N(p', s') | \mathcal{O}_V^{\mu\nu} | N(p, s) \rangle &= \bar{u}_N(p', s') \Lambda_{\mu\nu}^q(Q^2) u_N(p, s), \\ \Lambda_{\mu\nu}^q(Q^2) &= A_{20}^q(Q^2) \gamma^{\{\mu} P^{\nu\}} + B_{20}^q(Q^2) \frac{\sigma^{\{\mu\alpha} q_\alpha P^{\nu\}}}{2m} \\ &\quad + C_{20}^q(Q^2) \frac{1}{m} Q^{\{\mu} Q^{\nu\}}, \end{aligned} \quad (1)$$

with  $Q=p'-p$  the momentum transfer and  $P=(p'+p)/2$  the total momentum. The axial-vector operator is  $\mathcal{O}_A^\mu = \bar{q} \gamma_\mu \gamma_5 q$  and the one-derivative vector operator  $\mathcal{O}_V^{\mu\nu} = \bar{q} \gamma^{\{\mu} \overleftrightarrow{D}^{\nu\}} q$ , where the curly brackets in  $\mathcal{O}_V$  represent a symmetrization over pairs of indices and a subtraction of the trace.  $\Lambda_{\mu\nu}^q$  is decomposed in terms of three Lorentz invariant generalized form factors (GFFs)  $A_{20}^q(Q^2)$ ,  $B_{20}^q(Q^2)$  and  $C_{20}^q(Q^2)$ . A corresponding decomposition can also be made for the nucleon matrix element of the gluon operator  $\mathcal{O}_g^{\mu\nu}$ . The quark (gluon) total angular momentum can be written as  $J_{q(g)} = \frac{1}{2} [A_{20}^{q(g)}(0) + B_{20}^{q(g)}(0)]$ , while the average momentum fraction is determined from  $A_{20}^{q(g)}(0) = \langle x \rangle_{q(g)}$  and  $g_A^q \equiv \Delta \Sigma_q$  where  $g_A^q$  is the nucleon axial charge. While  $A_{20}^q(0)$  can be extracted directly at  $Q^2=0$ ,  $B_{20}^q(0)$  needs to be extrapolated to  $Q^2=0$  using the values obtained at finite  $Q^2$ .

We compute the gluon momentum fraction by considering the  $Q^2=0$  nucleon matrix element of the operator  $\mathcal{O}_g^{\mu\nu} = 2\text{Tr}[G_{\mu\sigma} G_{\nu\sigma}]$ , taking the combination  $\mathcal{O}_g \equiv \mathcal{O}_{44} - \frac{1}{3} \mathcal{O}_{jj}$ ,

$$\langle N(p, s') | \mathcal{O}_g | N(p, s) \rangle = \left( -4E_N^2 - \frac{2}{3} \vec{p}^2 \right) \langle x \rangle_g, \quad (2)$$

where we further take the nucleon momentum  $\vec{p}=0$ .

In lattice QCD the aforementioned nucleon matrix elements are extracted from a ratio,  $R_\Gamma(t_s, t_{\text{ins}})$ , of a three-point function  $G_\Gamma^{3\text{pt}}(t_s, t_{\text{ins}})$  constructed with an operator  $\Gamma$  coupled to a quark divided by the nucleon two-point functions  $G^{2\text{pt}}(t_s)$ , where  $t_{\text{ins}}$  is the time slice of the operator insertion relative to the time slice where a state with the quantum numbers of the nucleon is created (source). For sufficiently large time separations  $t_s - t_{\text{ins}}$  and  $t_{\text{ins}}$  the ratio  $R_\Gamma(t_s, t_{\text{ins}})$  yields the appropriate nucleon matrix element. To determine  $B_{20}(Q^2)$  we need the nucleon matrix element for  $Q^2 \neq 0$ , which can be extracted by defining an equivalent ratio as described in detail in Refs. [21–23]. An extrapolation of  $B_{20}(Q^2)$  is then carried out to obtain  $B_{20}(0)$ . We employ three approaches in order to check that the time separations  $t_s - t_{\text{ins}}$  and  $t_{\text{ins}}$  are sufficiently large to suppress higher energy states with the same quantum numbers with the nucleon. These are: i) *Plateau method*. Identify the range of  $t_{\text{ins}}$  for which the ratio  $R_\Gamma(t_s, t_{\text{ins}})$  becomes time-independent and perform a constant fit; ii) *Summation method*. Summing  $R_\Gamma(t_s, t_{\text{ins}})$  over  $t_{\text{ins}}$ , to yield  $\sum_{t_{\text{ins}}} R_\Gamma(t_s, t_{\text{ins}}) = R_\Gamma^{\text{summ}}(t_s) = C + t_s \mathcal{M} + \mathcal{O}(e^{-(E_1 - E_0)t_s}) + \dots$ , where  $C$  is a constant. The matrix element  $\mathcal{M}$  is then obtained from the slope of a linear fit with respect to  $t_s$ ; iii) *Two-state fit method*. We perform a simultaneous fit to the three- and two-point function varying  $t_{\text{ins}}$  for several values of  $t_s$  include the first excited state in the fit function. If excited states are suppressed, the plateau method should yield consistent values when increasing  $t_s$  within a sufficiently large  $t_s$ -range. We require that we observe convergence of the values extracted from the plateau method and additionally that these values are compatible with the results extracted from the two-state fit and the summation method. We take the difference between the plateau and two-state fit values as a systematic error due to residual excited states.

The three-point functions for the axial-vector and vector one-derivative operators entering the ratio  $R_\Gamma(t_s, t_{\text{ins}})$ , receive two contributions, one when the operator couples to the valence up and down quarks (so-called connected) and when it couples to sea quarks and gluons (disconnected). The connected contributions are computed by employing sequential inversion through the sink [24]. Disconnected diagrams are computationally very demanding, due to the fact that they involve a closed quark loop and thus a trace over the quark propagator. A feasible alternative is to employ stochastic techniques [25] to obtain an estimate of the all-to-all propagator needed for the evaluation of the closed quark loop. For the up and down quarks, we utilize *exact deflation* [26, 27], by computing the  $N_{ev}$  lowest eigenmodes of the Dirac matrix to precondition the conjugate gradient (CG) solver. Taking  $N_{ev}=500$  yields an improvement of about twenty times, compared to the standard conjugate gradient method. We also exploit the properties of the twisted mass action to improve our computation using

the so-called one-end trick [28, 29] that yields an increase in the signal-to-noise ratio [30, 31]. This also allows the evaluation of the quark loops for all insertion time-slices, and since the two-point function is computed for all  $t_s$ , the disconnected three-point function is obtained for any combination of  $t_s$  and  $t_{\text{ins}}$  allowing a thorough study of excited states effects. In addition, an improved approach is employed for  $\langle x \rangle_q$  exploiting the spectral decomposition of the Dirac matrix. Within this approach, we use the lowest eigenmodes to construct part of the all-to-all propagator in an *exact* manner. This allows us to invert less stochastic sources for constant variance, hence  $N_r$  is smaller for  $\langle x \rangle_q$  in Table I. The remaining part of the loop is calculated stochastically, with the use of the one-end trick.

For the heavier strange and charm quarks, the *truncated solver method* [32] (TSM) performs well [30, 31]. In the TSM an appropriately tuned large number of low-precision and a small number of high-precision stochastic inversions is combined to obtain an estimate of  $G_s(x; x)$ . We give the tuned parameters in Table I. These methods have been recently employed to compute other nucleon observables using this ensemble [33–35] as well as at higher than physical pion masses [30, 31].

The three-point function of the gluon operator is purely disconnected. To overcome the low signal-to-noise ratio we apply stout smearing to the gauge links entering the gluonic operator  $\mathcal{O}_g^{\mu\nu}$  [36]. Use of an analytic link smearing is essential for performing the perturbative computation of the renormalization. Using smearing and a total of 209400 measurements we obtain the bare matrix element to a few percent accuracy [11]. We note that a non-zero gluon momentum in the quenched approximation was found in Ref. [37].

In Table I we summarize the statistics used for the calculation for both quark and gluon observables.

Connected			Disconnected				
$t_s/a$	$N_{\text{cfg}}$	$N_{\text{src}}$	Observable	$N_{\text{cfg}}$	$N_{\text{src}}$	$N_r^{HP}$	$N_r^{LP}$
10,12,14	579	16	light, $g_A$	2136	100	2250	0
16	542	88	light, $\langle x \rangle_q$	1219	100	1000	0
18	793	88	strange, $g_A$	2153	100	63	1024
			strange, $\langle x \rangle_q$	2153	100	30	960
			gluon, $\langle x \rangle_g$	2094	100	-	-

TABLE I: Statistics used in this calculation.  $t_s$  is the sink time separation relative to the source which is used for the connected three-point functions.  $N_{\text{cfg}}$  is the number of configurations and  $N_{\text{src}}$  the number of source positions per configuration.  $N_r^{HP}$  ( $N_r^{LP}$ ) is the number of high- (low-) precision stochastic vectors used for the quark loops.

*Renormalization:* We determine the renormalization functions for the axial-vector charge and one-derivative vector operators non-perturbatively, in the RI'-MOM scheme. We employ a momentum source and perform a perturbative subtraction of  $\mathcal{O}(g^2 a^\infty)$ -terms [38, 39].

This subtracts the leading cut-off effects yielding only a weak dependence of the renormalization factors on the renormalization scale  $(ap)^2$  for which the  $(ap)^2 \rightarrow 0$  limit can be reliably taken. Lattice QCD results for both the isovector and isoscalar axial charge are renormalized non-perturbatively with  $Z_A^{\text{isovector}}=0.7910(4)(5)$  and  $Z_A^{\text{isoscalar}}=0.7968(25)(91)$  respectively [35, 38]. The one-derivative vector operator is non-perturbatively renormalized with  $Z_{DV}=1.1251(27)(17)$  in the  $\overline{\text{MS}}$ -scheme at 2 GeV [38]. The renormalization of the gluon operator is carried out perturbatively. Being a flavor singlet operator, it mixes with other operators and in particular the quark singlet operator. Due to this mixing, appropriate renormalization conditions require computation of more than one matrix element. We perform the computation in one-loop lattice perturbation theory and use the action parameters that coincide with the ensemble of this work. To avoid the introduction of an intermediate RI-type scheme, we define a convenient renormalization prescription that utilizes both dimensional and lattice regularization results (see Ref. [11] for more details).

The physical result of the gluon momentum fraction can be related to the bare matrix elements  $\langle x \rangle_g^{\text{bare}}$  and  $\langle x \rangle_q^{\text{bare}}$  using  $\langle x \rangle_g = Z_{gg} \langle x \rangle_g^{\text{bare}} + Z_{gq} \sum_q \langle x \rangle_q^{\text{bare}}$ , where  $Z_{gg}$  and  $Z_{gq}$  are computed to one-loop. We note that the mixing coefficient  $Z_{gq}$  is a fraction of the statistical errors on our results. Therefore, for the quark momentum fractions, we renormalize with the non-perturbatively determined renormalization factor, neglecting the mixing with the gluon operator. We note that the perturbative and non-perturbative renormalization functions  $Z_{DV}$  differ by 10%, which is a much larger effect than the mixing.

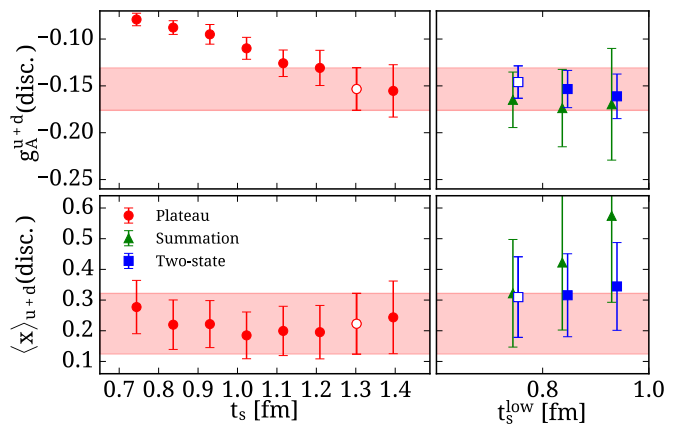


FIG. 1: The disconnected sea quark contribution (denoted by disc.) to the isoscalar axial charge (upper) and momentum fraction (lower) as a function of the sink-source time separation  $t_s$  for the plateau method (circles) and as a function of the lower time value of  $t_s$  used in the fits for the summation (green triangles) and two-state fit (blue square) methods. The open circle indicates the final value and the band its statistical error, while the open square is the value taken to determine the systematic error due to excited state contamination.

In Fig. 1 we show the result of the three analyses carried out to extract the disconnected contribution to the isoscalar axial charge  $g_A^{u+d}$  and quark momentum fraction  $\langle x \rangle_{u+d}$ . Taking the value at  $t_s=14a=1.3$  fm is consistent with the result from the two-state fit and summation method, for both quantities. We take the plateau value at  $t_s=14a$  as our final result and assign as systematic error due to excited states the difference between this value and the mean value determined from the two-state fit. The same analysis is performed for the strange and charm disconnected contributions. The analysis for the valence quark contributions at lower statistics was presented in Ref. [40] and it is followed also here.

*Results:* In Fig. 2 we present our results on the up, down and strange quark contributions to the nucleon axial charge that yield the quark intrinsic spin contributions to the nucleon spin. Since we are using a single ensemble we cannot directly assess finite volume and lattice spacings effects. However, previous studies carried out using  $N_f=2$  and  $N_f=2+1+1$  twisted mass fermion (TMF) ensembles at heavier than physical pion masses for the connected contributions allow us to assess cut-off and volume effects [21, 41]. In Fig. 2 we include TMF results for  $N_f=2$  ensembles at  $m_\pi \sim 465$  MeV one with lattice spacing  $a=0.089$  fm and one with  $a=0.07$  fm with similar spatial lattice length  $L$ , as well as, at  $m_\pi=260$  MeV, one with  $a=0.089$  fm and another with  $a=0.056$  fm and similar  $L$ . At both pion masses the results are in complete agreement as we vary the lattice spacing from 0.089 fm to 0.056 fm pointing to cut-off effects smaller than our statistical errors. For assessing finite volume effects we compare two  $N_f=2$  ensembles both with  $a=0.089$  fm and  $m_\pi \sim 300$  MeV, but one with  $m_\pi L=3.3$  and the other with  $m_\pi L=4.3$ . The values are completely compatible showing that volume effects are also within our statistical errors. To assess possible strange quenching effects we compare in Fig. 2 results for the connected contributions using  $N_f=2$  and  $N_f=2+1+1$  TMF ensembles both at  $m_\pi \sim 375$  MeV and find very good agreement [51]. The latter is a high statistics analysis yielding very small errors. We note, however, that the limited accuracy of the  $N_f=2$  result would still allow a quenching effect of the order of its statistical error and only an accurate calculation using  $N_f=2+1+1$  simulations at the physical point would be able to resolve this completely. In Fig. 2, we also compare recent lattice QCD results on the strange intrinsic spin,  $\frac{1}{2}\Delta\Sigma_s$ , at heavier than physical pion masses and find agreement among lattice QCD results, indicating that lattice artifacts are within the current statistical errors. We note, in particular, that all lattice QCD results yield a non-zero and negative strange quark intrinsic spin contribution  $\frac{1}{2}\Delta\Sigma_s$ . We also compute the charm axial charge and momentum fraction, at the physical point, and find that both are consistent with zero.

To determine the total quark angular momentum  $J_q$ , we need, beyond  $A_{20}^q(0)$ , the generalized form factor

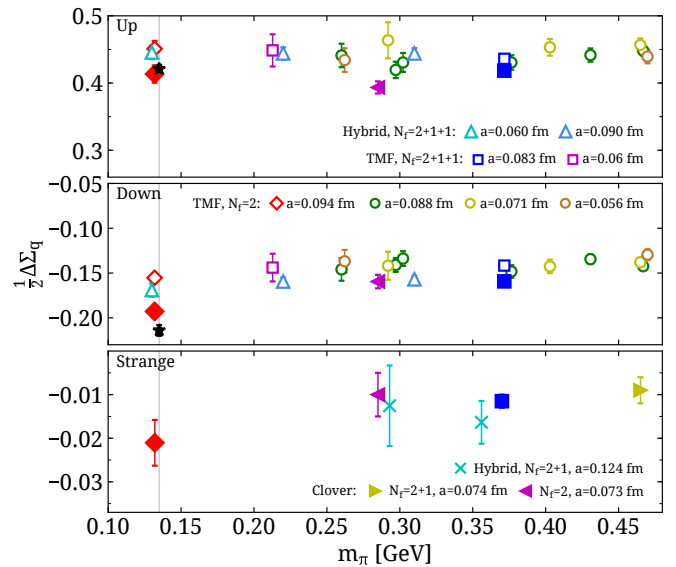


FIG. 2: The up (upper), down (center) and strange (lower) quark intrinsic spin contributions to the nucleon spin versus the pion mass. Open symbols show results with only connected contributions while filled symbols denote both connected and disconnected contributions using the same ensemble as the one for the connected only. Red diamonds are the results of this work. Circles are  $N_f=2$  results, and squares are  $N_f=2+1+1$  [30, 31, 41] by ETMC. We compare with lattice QCD results from other  $\mathcal{O}(a)$ -improved actions from Refs. [42] (filled magenta triangle) by QCDSF, [43] (light blue cross) and [44] by CSSM/QCDSF (yellow filled right triangle). We also show results using a hybrid action from PNDME [45] (open blue triangles). Experiment is denoted by the black asterisks [46, 47].

$B_{20}^q(0)$ , which is extracted from the nucleon matrix element of the vector one-derivative operator for  $Q^2 \neq 0$  as described in Ref. [21]. For the isovector case, we find  $B_{20}^{u-d}(0)=0.313(19)$ , and for the isoscalar connected contribution  $B_{20}^{u+d, \text{conn.}}(0)=0.012(20)$ . We observe that the latter is consistent with zero, as is the disconnected contribution  $B_{20}^{u+d, \text{disc.}}(Q^2=0.074 \text{ GeV}^2)$ . Similarly, the strange and charm  $B_{20}^{s,c}(Q^2)$  are zero, which implies  $J_{s,c}=\frac{1}{2}\langle x \rangle_{s,c}$ . In what follows we will also take the gluon  $B_{20}^g(0)$  to be zero and thus  $J_g=\frac{1}{2}\langle x \rangle_g$ .

Our final values for the quark total and angular momentum contributions are given in Table II. The value of  $\langle x \rangle_{u-d}=0.194(9)(11)$  is on the upper bound as compared to the recent phenomenological value extracted in Ref. [7]. Determinations of  $\langle x \rangle_{u-d}$  within lattice QCD using simulations with larger than physical pion masses have yielded larger values, an effect that is partly understood to be due to contribution of excited states to the ground state matrix element [48]. We note that our value is in agreement with that determined by RQCD using  $N_f=2$  clover fermions at pion mass of 151 MeV [49] and that lattice QCD results on  $\langle x \rangle_{u-d}$  and  $J_{u-d}$  for ensembles with larger than physical pion masses including

TABLE II: Our results for the intrinsic spin ( $\frac{1}{2}\Delta\Sigma$ ), angular ( $L$ ) and total ( $J$ ) momentum contributions to the nucleon spin and to the nucleon momentum  $\langle x \rangle$ , in the  $\overline{\text{MS}}$ -scheme at 2 GeV, from up (u), down (d) and strange (s) quarks and from gluons (g), as well as the sum of all contributions (tot.), where the first error is statistical and the second a systematic due to excited states.

	$\frac{1}{2}\Delta\Sigma$	$J$	$L$	$\langle x \rangle$
u	0.415(13)(2)	0.308(30)(24)	-0.107(32)(24)	0.453(57)(48)
d	-0.193(8)(3)	0.054(29)(24)	0.247(30)(24)	0.259(57)(47)
s	-0.021(5)(1)	0.046(21)(0)	0.067(21)(1)	0.092(41)(0)
g	-	0.133(11)(14)	-	0.267(22)(27)
tot.	0.201(17)(5)	0.541(62)(49)	0.207(64)(45)	1.07(12)(10)

ours are in overall agreement [41]. Results within lattice QCD for the individual quark  $\langle x \rangle_q$  and  $J_q$  contributions are scarce. The current computation is the first one using dynamical light quarks with physical masses. A recent quenched calculation yielded values of  $\langle x \rangle_{u,d}$  consistent with ours.

In Fig. 3 we show schematically the various contributions to the spin and momentum fraction. Using a different approach to ours, the gluon helicity was recently computed within lattice QCD and found to be 0.251(47)(16) [8]. Although we instead compute the gluon total angular momentum and the two approaches have different systematic uncertainties, we both find non-negligible gluon contributions to the proton spin.

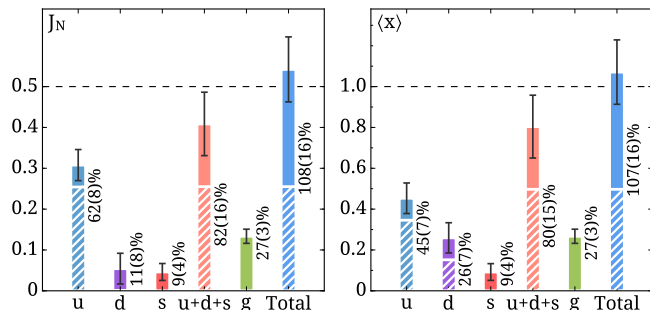


FIG. 3: Left: Nucleon spin decomposition. Right: Nucleon momentum decomposition. All quantities are given in the  $\overline{\text{MS}}$ -scheme at 2 GeV. The striped segments show valence quark contributions (connected) and the solid segments the sea quark and gluon contributions (disconnected).

*Conclusions:* In this work we present a calculation of the quark and gluon contributions to the proton spin, directly at the physical point.

Having a single ensemble, we can only assess lattice systematic effects due to the quenching of the strange quark, the finite volume and the lattice spacing indirectly from other twisted mass ensembles. A direct evaluation of these systematic errors is currently not possible and will be carried out in the future. Individual components are computed for the up,

down, strange and charm quarks, including both connected (valence) and disconnected (sea) quark contributions. Our final numbers are collected in Table II. The quark intrinsic spin from connected and disconnected contributions is  $\frac{1}{2}\Delta\Sigma_{u+d+s}=0.299(12)(3)|_{\text{conn.}} - 0.098(12)(4)|_{\text{disc.}}=0.201(17)(5)$ , while the total quark angular momentum is  $J_{u+d+s}=0.255(12)(3)|_{\text{conn.}} + 0.153(60)(47)|_{\text{disc.}}=0.408(61)(48)$ . Our result for the intrinsic quark spin contribution agrees with the upper bound set by a recent phenomenological analysis of experimental data from COMPASS [50], which found  $0.13 < \frac{1}{2}\Delta\Sigma < 0.18$ . Using the spin sum one would deduce that  $J_g=\frac{1}{2}-J_q=0.092(61)(48)$ , which is consistent with taking  $J_g=\frac{1}{2}\langle x \rangle_g=0.133(11)(14)$  via the direct evaluation of the gluon momentum fraction, which suggests that  $B_{20}^g(0)$  is indeed small. Furthermore, we find that the momentum sum is satisfied  $\sum_q \langle x \rangle_q + \langle x \rangle_g=0.497(12)(5)|_{\text{conn.}} + 0.307(121)(95)|_{\text{disc.}} + 0.267(12)(10)|_{\text{gluon}}=1.07(12)(10)$  as is the spin sum of quarks and gluons giving  $J_N=\sum_q J_q + J_g=0.408(61)(48) + 0.133(11)(14)=0.541(62)(49)$  resolving a long-standing puzzle.

*Acknowledgments:* We thank all members of ETMC for an enjoyable collaboration and in particular Fernanda Steffens for fruitful discussions. We acknowledge funding from the European Union's Horizon 2020 research and innovation program under the Marie Skłodowska-Curie grant agreement No 642069. M. C. acknowledges financial support by the National Science Foundation under Grant No. PHY-1714407. This work used computational resources from the Swiss National Supercomputing Centre (CSCS) under project IDs s540, s625 and s702, from the John von Neumann-Institute for Computing on the Jureca and the BlueGene/Q Juqueen systems at the research center in Jülich from a Gauss allocation on SuperMUC with ID 44060.

- [1] J. Ashman et al. (European Muon), Phys. Lett. **B206**, 364 (1988).
- [2] J. Ashman et al. (European Muon), Nucl. Phys. **B328**, 1 (1989).
- [3] C. A. Aidala, S. D. Bass, D. Hasch, and G. K. Mallot, Rev. Mod. Phys. **85**, 655 (2013), 1209.2803.
- [4] A. Adare et al. (PHENIX), Phys. Rev. **D90**, 012007 (2014), 1402.6296.
- [5] P. Djawotho (STAR), Nuovo Cim. **C036**, 35 (2013), 1303.0543.
- [6] D. de Florian, R. Sassot, M. Stratmann, and W. Vogelsang, Phys. Rev. Lett. **113**, 012001 (2014), 1404.4293.
- [7] S. Alekhin, J. Blmlin, S. Moch, and R. Placakyte (2017), 1701.05838.
- [8] Y.-B. Yang, R. S. Sufian, A. Alexandru, T. Draper, M. J. Glatzmaier, K.-F. Liu, and Y. Zhao, Phys. Rev. Lett. **118**, 102001 (2017), 1609.05937.
- [9] C. Alexandrou, M. Constantinou, K. Hadjiyiannakou,

- C. Kallidonis, G. Koutsou, K. Jansen, C. Wiese, and A. V. Avils-Casco, PoS **LATTICE2016**, 153 (2016), 1611.09163.
- [10] C. Alexandrou, M. Constantinou, K. Hadjiyiannakou, C. Kallidonis, G. Koutsou, K. Jansen, H. Panagopoulos, F. Steffens, A. Vaquero, and C. Wiese, PoS **DIS2016**, 240 (2016), 1609.00253.
- [11] C. Alexandrou, M. Constantinou, K. Hadjiyiannakou, K. Jansen, H. Panagopoulos, and C. Wiese (2016), 1611.06901.
- [12] C. Alexandrou, EPJ Web Conf. **137**, 01004 (2017), 1612.04644.
- [13] M. Constantinou, in *SPIN 2016* (2017), 1701.02855.
- [14] R. Frezzotti, P. A. Grassi, S. Sint, and P. Weisz (Alpha), JHEP **08**, 058 (2001), hep-lat/0101001.
- [15] R. Frezzotti and G. C. Rossi, JHEP **08**, 007 (2004), hep-lat/0306014.
- [16] A. Abdel-Rehim et al. (ETM) (2015), 1507.05068.
- [17] C. Alexandrou and C. Kallidonis (2017), 1704.02647.
- [18] K. Osterwalder and E. Seiler, Annals Phys. **110**, 440 (1978).
- [19] R. Frezzotti and G. C. Rossi, JHEP **10**, 070 (2004), hep-lat/0407002.
- [20] X.-D. Ji, Phys. Rev. Lett. **78**, 610 (1997), hep-ph/9603249.
- [21] C. Alexandrou, J. Carbonell, M. Constantinou, P. A. Harraud, P. Guichon, K. Jansen, C. Kallidonis, T. Korzec, and M. Papinutto, Phys. Rev. **D83**, 114513 (2011), 1104.1600.
- [22] C. Alexandrou, M. Brinet, J. Carbonell, M. Constantinou, P. A. Harraud, P. Guichon, K. Jansen, T. Korzec, and M. Papinutto, Phys. Rev. **D83**, 094502 (2011), 1102.2208.
- [23] C. Alexandrou, M. Brinet, J. Carbonell, M. Constantinou, P. A. Harraud, P. Guichon, K. Jansen, T. Korzec, and M. Papinutto (ETM), Phys. Rev. **D83**, 045010 (2011), 1012.0857.
- [24] G. Martinelli and C. T. Sachrajda, Nucl. Phys. **B316**, 355 (1989).
- [25] K. Bitar, A. D. Kennedy, R. Horsley, S. Meyer, and P. Rossi, Nucl. Phys. **B313**, 377 (1989).
- [26] G. S. Bali, H. Neff, T. Duessel, T. Lippert, and K. Schilling (SESAM), Phys. Rev. **D71**, 114513 (2005), hep-lat/0505012.
- [27] H. Neff, N. Eicker, T. Lippert, J. W. Negele, and K. Schilling, Phys. Rev. **D64**, 114509 (2001), hep-lat/0106016.
- [28] C. Michael and C. Urbach (ETM), PoS **LAT2007**, 122 (2007), 0709.4564.
- [29] C. McNeile and C. Michael (UKQCD), Phys. Rev. **D73**, 074506 (2006), hep-lat/0603007.
- [30] C. Alexandrou, M. Constantinou, V. Drach, K. Hadjiyiannakou, K. Jansen, G. Koutsou, A. Strelchenko, and A. Vaquero, Comput. Phys. Commun. **185**, 1370 (2014), 1309.2256.
- [31] A. Abdel-Rehim, C. Alexandrou, M. Constantinou, V. Drach, K. Hadjiyiannakou, K. Jansen, G. Koutsou, and A. Vaquero, Phys. Rev. **D89**, 034501 (2014), 1310.6339.
- [32] G. S. Bali, S. Collins, and A. Schafer, Comput. Phys. Commun. **181**, 1570 (2010), 0910.3970.
- [33] A. Abdel-Rehim, C. Alexandrou, M. Constantinou, K. Hadjiyiannakou, K. Jansen, C. Kallidonis, G. Koutsou, and A. Vaquero Aviles-Casco (ETM), Phys. Rev. Lett. **116**, 252001 (2016), 1601.01624.
- [34] C. Alexandrou et al., Phys. Rev. **D95**, 114514 (2017), 1703.08788.
- [35] C. Alexandrou, M. Constantinou, K. Hadjiyiannakou, K. Jansen, C. Kallidonis, G. Koutsou, and A. Vaquero Aviles-Casco (2017), 1705.03399.
- [36] C. Morningstar and M. J. Peardon, Phys. Rev. **D69**, 054501 (2004), hep-lat/0311018.
- [37] M. Deka et al., Phys. Rev. **D91**, 014505 (2015), 1312.4816.
- [38] C. Alexandrou, M. Constantinou, and H. Panagopoulos (ETM), Phys. Rev. **D95**, 034505 (2017), 1509.00213.
- [39] C. Alexandrou, M. Constantinou, T. Korzec, H. Panagopoulos, and F. Stylianou, Phys. Rev. **D83**, 014503 (2011), 1006.1920.
- [40] A. Abdel-Rehim et al., Phys. Rev. **D92**, 114513 (2015), [Erratum: Phys. Rev.D93,no.3,039904(2016)], 1507.04936.
- [41] C. Alexandrou, M. Constantinou, S. Dinter, V. Drach, K. Jansen, C. Kallidonis, and G. Koutsou, Phys. Rev. **D88**, 014509 (2013), 1303.5979.
- [42] G. S. Bali et al. (QCDSF), Phys. Rev. Lett. **108**, 222001 (2012), 1112.3354.
- [43] M. Engelhardt, Phys. Rev. **D86**, 114510 (2012), 1210.0025.
- [44] A. J. Chambers et al., Phys. Rev. **D92**, 114517 (2015), 1508.06856.
- [45] T. Bhattacharya, V. Cirigliano, S. Cohen, R. Gupta, H.-W. Lin, and B. Yoon, Phys. Rev. **D94**, 054508 (2016), 1606.07049.
- [46] A. Airapetian et al. (HERMES), Phys. Rev. **D75**, 012007 (2007), hep-ex/0609039.
- [47] J. Blumlein and H. Bottcher, Nucl. Phys. **B841**, 205 (2010), 1005.3113.
- [48] G. S. Bali, S. Collins, M. Deka, B. Glässle, M. Göckeler, J. Najjar, A. Nobile, D. Pleiter, A. Schäfer, and A. Sternbeck, Phys. Rev. **D86**, 054504 (2012), 1207.1110.
- [49] G. S. Bali, S. Collins, B. Glässle, M. Göckeler, J. Najjar, R. H. Rdl, A. Schäfer, R. W. Schiel, A. Sternbeck, and W. Söldner, Phys. Rev. **D90**, 074510 (2014), 1408.6850.
- [50] C. Adolph et al. (COMPASS), Phys. Lett. **B753**, 18 (2016), 1503.08935.
- [51] We find  $\frac{1}{2}\Delta\Sigma_u=0.431(11)$  and  $\frac{1}{2}\Delta\Sigma_d=-0.148(7)$  for the  $N_f=2$  ensemble consistent with  $\frac{1}{2}\Delta\Sigma_u=0.436(2)$  and  $\frac{1}{2}\Delta\Sigma_d=-0.142(1)$  for the  $N_f=2+1+1$  ensemble.